
LANDSLIDE TOPOLOGY UNCOVERS FAILURE MOVEMENTS

Kamal Rana^{1,2,3,†,*}, Kushanav Bhuyan^{4,†,*}, Joaquin Vicente Ferrer^{3,5}, Fabrice Cotton^{2,6}, Ugur Ozturk^{2,3}, Filippo Catani⁴, and Nishant Malik⁷

¹Chester F. Carlson Center for Imaging Science, Rochester Institute of Technology, Rochester, 14623, NY, USA

²Helmholtz Centre Potsdam – GFZ German Research Centre for Geosciences, Potsdam, 14473, Brandenburg, Germany

³Institute of Environmental Science and Geography, University of Potsdam, Potsdam, 14473, Brandenburg, Germany

⁴Machine Intelligence and Slope Stability Laboratory, Department of Geosciences, University of Padova, Padua, 35129, Veneto, Italy

⁵Potsdam Institute for Climate Impact Research, Potsdam, 14473, Brandenburg, Germany

⁶Institute of Geosciences, University of Potsdam, Potsdam, 14473, Brandenburg, Germany

⁷School of Mathematical Sciences, Rochester Institute of Technology, Rochester, 14623, NY, USA

[†]These authors contributed equally and share first authorship.

ABSTRACT

The death toll and monetary damages from landslides continue to rise despite advancements in predictive modeling. The predictive capability of these models is limited as landslide databases used in training and assessing the models often have crucial information missing, such as underlying failure types. Here, we present an approach for identifying failure types based on their movements, e.g., slides and flows by leveraging 3D landslide topology. We observe topological proxies reveal prevalent signatures of mass movement mechanics embedded in the landslides' morphology or shape, such as detecting coupled movement styles within complex landslides. We find identical failure types exhibit similar topological properties, and by using them as predictors, we can identify failure types in historic and event-specific landslide databases (including multi-temporal) from various geomorphological and climatic contexts such as Italy, the US's Pacific Northwest region, Denmark, Turkey, and China with 80-94% accuracy. To demonstrate the real-world application of the method, we implement it in two undocumented datasets from China and publicly release the datasets. These new insights can considerably improve the performance of landslide predictive models and impact assessments. Moreover, our work introduces a new paradigm for studying landslide shapes to understand underlying processes through the lens of landslide topology.

Keywords Topological Data Analysis · Landslide failure movements · Machine Learning · Point cloud classification

1 Introduction

Every year, landslides cause economic damages worth 20 billion US dollars [1], and between 2004 and 2019 non-seismic landslides alone caused about 70,000 fatalities worldwide [2]. Within the first two months of 2023, we have seen reports of devastating landslides in São Paulo, Brazil [3], Southern Peru [4], and New Zealand [5], injuring many and killing approximately 70 people. Adding to this, recent studies count over one million landslide occurrences with annual volumes estimated at fifty-six billion cubic meters globally [6], presenting a risk to sixty million people [7]. With the increase in urbanization, global climate change, and environmental change trends, the frequency of landslides and the associated risks will keep increasing globally over time [7]. In line with this, landslides are anticipated to evolve and remobilize with increased frequency under changing climatic conditions on a decadal scale [8, 9]. Our ability to identify hazards from emerging landslides and dynamically assess impact areas is essential in averting risk to rapidly urbanizing communities and adapting to changing environmental conditions [10, 7].

To address the rising landslide risk, predictive models for hazard, risk, and early warning systems are developed which assist in forecasting landslide occurrences and locating landslide-prone regions to mitigate the associated impacts [11]. However, the efficacy of these models is contingent on the quality of the underlying landslide databases. These

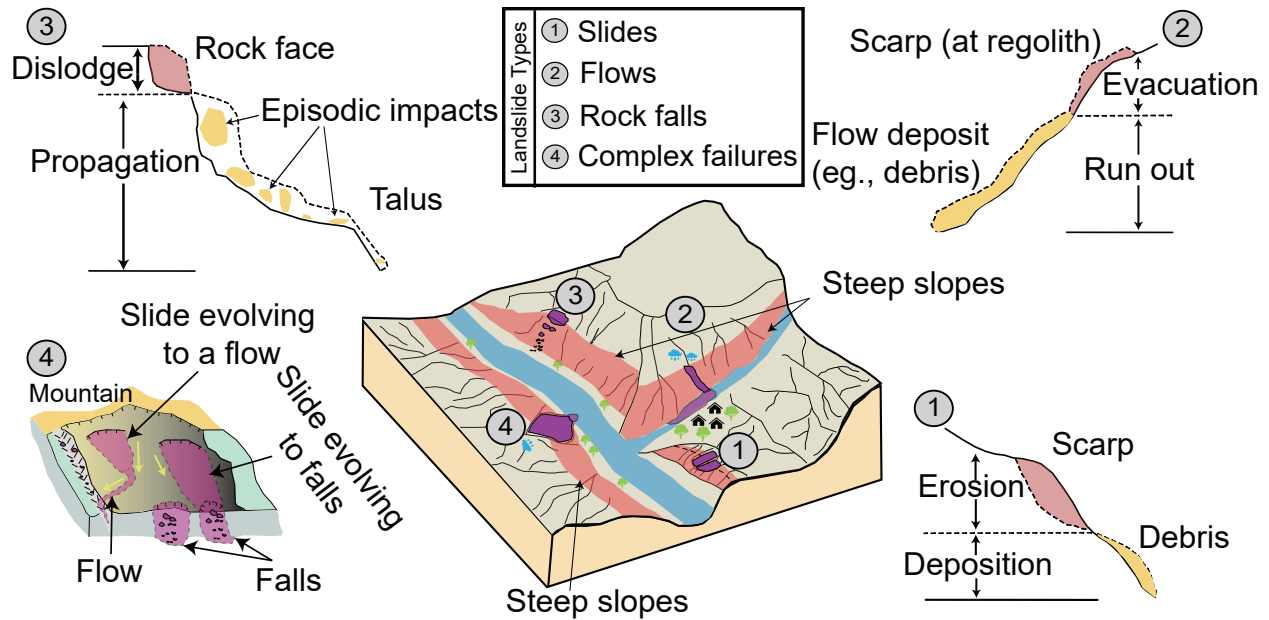


Figure 1: The schematic broadly illustrates different landslide failure types and their associated mechanical and kinematic behavior, excluding sub-type movements. For example, Type 1 refers to slide-type failures that can constitute deep ruptures, where a cohesive unit of soil or rock slides down a slope following a well-defined rupture plane. Type 2 refers to flow-type failures where soil, rock, or other material travels down a slope as a dense, fluid-like mass with a flow-like motion. Type 3 is a fall-type of failure where a body of rock detaches from a steep slope or cliffs and exhibits free falling and episodic impacts as it propagates down the slope. Type 4 refers to the complex interaction and effect of numerous geomorphic processes transpiring in a single failure event, where processes start as one types and evolve into another; such as a slide-type failure evolving to a flow-type failure.

databases often lack the much-needed information about the type of failure of the mapped landslides [12]. Generally, these databases include a broader definition of landslides that covers all types of gravitational mass wasting processes, such as slides, flows, and falls including sub-types based on their movement, e.g., rotational slides [13] combined together, thereby hampering the capability of predictive models. Typically, each landslide failure type exhibits different geological, geometrical, and geotechnical properties (see Figure 1). For instance, slides have conspicuous primary scarps and collapse along the planar or rotational surfaces [14], flows such as mudflows exhibit visco-plastic or viscous/fluid kinematics caused by excess pore water pressure [15], and rock falls entails the free falling of fragmented rocks from steep slopes [16] (see Supplementary Section S2 for detailed explanations). Practitioners usually combine these different failure movements into one group within an inventory, despite their different properties [17, 18, 19], since categorizing them manually requires comprehensive surveys (remote and field) and standardized classification protocols [12], which are laborious and time-consuming. Consequently, predictive models start to harbor significant levels of uncertainty and bias [20], hence failing to match empirical observations, especially when moving from local levels to regional and global scales [21, 22, 23].

Preliminary attempts at identifying failure movement types have considered both knowledge-driven and data-driven approaches. While the former are region-specific, bounded by expert-based rules, and constrained to small areas [24, 25], the latter addressed these problems with supervised learning and have successfully identified landslide failure types in the Italian context [26]. However, the existing solutions are still limited in their prediction capabilities, as the failure information is derived from geometric properties of two-dimensional (2D) landslide polygons (outlining the landslide planforms). Owing to the inherent limitations of 2D landslide polygons, crucial kinematic and mechanical details embedded in the landslides' three-dimensional (3D) morphology are overlooked, such as the style of kinematic progression, deformation patterns and structures, and debris deposits. Furthermore, the complex kinematic evolution of one or more failure types may culminate in the convergent evolution of landslide shapes, wherein landslides starting as completely different movements may evolve to follow similar planar outlines. This presents challenges in deducing failure types solely based on 2D geometric descriptors or rudimentary topographic metrics. We argue that these overlooked kinematic attributes are intricately linked with the 3D morphological properties of landslides, which can be comprehensively analyzed through topological methods.

Topology is a sub-discipline of mathematics explored in many fields that concern the study of shapes [27], such as in protein structures, data modeling, complex networks, and signal processing [28, 29, 30, 31]. We explore advanced data analysis tools rooted in topology, known as topological data analysis (TDA), which captures critical structures present in the data’s shape (in our case, the landslide’s 3D shape). We hypothesize that key features of landslide kinematics are embedded in the 3D topology of the involved landforms and that TDA properties can capture their kinematic movements as a proxy for identifying landslide failures.

In this study, we introduce an approach for uncovering landslide failure types based on their mode of movement by examining the topological properties inherent in the 3D shapes of landslides. We develop the method using the Italian historical inventory from IFFI and then deploy it to landslide inventories from varying geomorphological and climatic settings: the United States (US) Pacific Northwest region, Denmark, Turkey, and China (see Figure 2) to validate the effectiveness and applicability of the approach. We demonstrate that this method offers a more comprehensive understanding of the underlying failure types compared to traditional analyses based on 2D polygonal geometry. We also explore the model’s ability to identify sub-types of the failure movements (e.g., translational and rotational slides, earth and debris flow). Also, we utilized the topological properties of complex landslides to reveal coupled failure types underlying the formation of complex landslides. In addition, we identify the types of failure in an event-based multi-temporal landslide inventory, enhancing our understanding of landslide dynamics and behaviors in real-world scenarios. Moreover, we deployed our method on two undocumented (paleo-event) datasets as a real-world application, which we verified using Google Earth archive imageries. To the best of our knowledge, sub-type failure movements, temporal prediction of failure movements, and detection of the underlying failure types within complex landslides have never been investigated using an automated data-driven approach. Here, we showcase with our findings that the proposed method (1) is user-friendly, exclusively requiring only the landslide polygonal shape and a Digital Elevation Model (DEM) as input, (2) exhibits high performance in discerning failure types based on their movements, (3) is transferable across various geomorphological and climatic regions, and (4) shows strong performance and remains robust, even when the availability of samples is limited, indicating its wide applicability in data-scarce regions. By offering a deeper understanding of landslide failure movements, this approach has the potential to enhance the accuracy and reliability of landslide susceptibility, hazard, and risk assessment models, by providing valuable insights to the predictive modeling community.

2 Methods

2.1 Topological Feature Engineering

In the proposed method, landslide polygons serve as the primary input. These polygons represent the 2D outline of the landslide body on the ground and are commonly found in landslide databases. Each vertex of the landslide polygon comprises geographical latitude and longitude coordinates. Utilizing the Digital Elevation Model, the landslide polygons are transformed into normalized 3D shape outlines, wherein each vertex encompasses latitude, longitude, and elevation information. Topological Data Analysis (TDA) is employed to extract the geometrical and topological characteristics of a landslide’s 3D shape outline (see Figure 4). This information is subsequently used as input for a machine learning algorithm, specifically the random forest. The Python library Giotto-TDA is leveraged to extract an assortment of TDA properties/features from the 3D shape of landslides [33]. To ascertain the most pertinent features for landslide-type classification, a correlation test is conducted between TDA features, and those with high correlation are removed. The remaining, less correlated features are then assessed, and the least important ones are iteratively eliminated until six robust predictors remain. The exclusion of additional predictors results in decreased performance, while incorporating more than seven yields comparable outcomes. Utilizing fewer predictors facilitates the development of a more generalizable model. The six features thus form a feature space for the random forest classifier.

Topological Data Analysis (TDA) quantifies the multidimensional shape of data using algebraic topology techniques. TDA offers a variety of metrics for capturing the geometric and topological properties of data shape [34]. These metrics could be used as a feature space for the machine learning algorithm to solve various classification and regression problems, such as shape classification. TDA’s central idea is persistent homology, which identifies persistent geometric features by using simplicial complexes to extract topological features from point cloud data. Simplicial complexes are a collection of simplexes that are the building blocks of higher-dimensional counterparts of a graph. An n -dimensional simplex is formed by connecting $n+1$ affinely independent points [35, 36]. For example, a point is a 0-dimensional simplex, an edge that connects two points is a 1-dimensional simplex, and a filled triangle formed by combining three non-linear points is a 2-dimensional simplex. A Vietoris-Rips complex indicates the simplicial complex in the data’s shape using a parameter ϵ . The main idea of the Vietoris-Rips complex is to connect any two points in the point cloud data set whose distance is less than ϵ . These connections of data points create structures in the data that change with the parameter ϵ . Therefore, to get complete information about all the structures in the data, the idea is to use all $\epsilon > 0$ values.

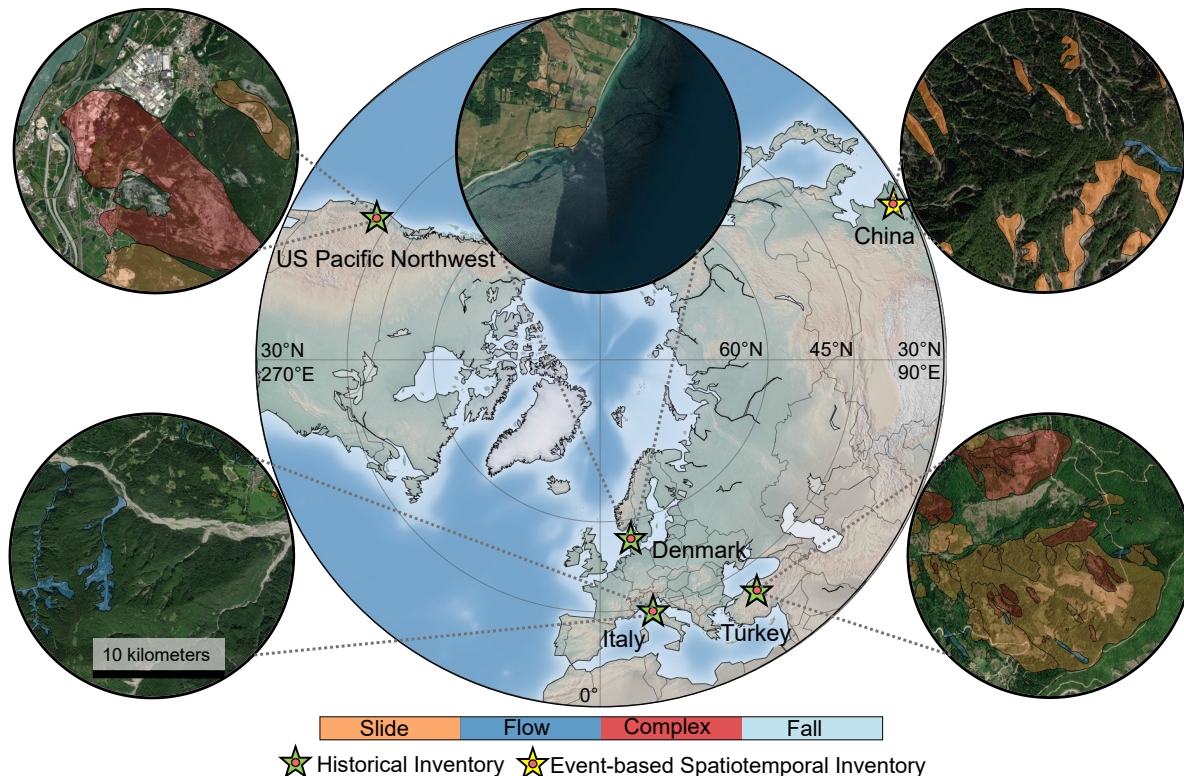


Figure 2: The diagram shows the geographical regions: Italy, the US Pacific Northwest, Turkey, Denmark, and China whose data we analyzed in this work. The inset in the circular shape shows snippets from diverse regions with landslide polygons of different failure movements on top of the World Imagery from ESRI. Map credits: Esri, Maxar, Earthstar Geographics, and the GIS User Community [32]

Only specific structures in the data shape provide crucial information about the geometrical and topological properties of the data. Homology measures these unique structures in the data, where e.g., 0-dimensional homology captures connected components or clusters, 1-dimensional homology measures loops, and 2-dimensional homology measures voids [35, 37]. These crucial structures emerge and die with changes in ϵ , and this information is captured in the persistence diagram. With the help of a persistence diagram, we can calculate various measures quantifying the topological properties of the shape—persistence entropy, average lifetime, number of points, Betti curve-based measure, persistence landscape curve-based measure, Wasserstein amplitude, Bottleneck amplitude, Heat kernel-based measure, and landscape image-based measure [38, 39, 40]. We have explained all these topological features in detail in Supplementary Section S3. Finally, we used all these measures as input in the machine learning method—random forest.

2.2 Machine learning model: Random Forest

Random forest is an ensemble-based learning method that has shown promising results in various classification and regression problems [41, 42, 43, 44, 45]. Random forest classifiers consist of multiple classifiers trained independently on bootstrapping training samples. Bootstrapping N training samples leads to $\frac{2N}{3}$ independent samples, so each tree in the random forest is constructed from a distinct subset of training samples [46, 47]. Moreover, each tree in the random forest predicts the output class of the testing sample independently, and the class with the majority votes is the final decision of the random forest [48, 47].

Each random forest tree divides a parent node into two daughter nodes, right (r) and left (l). For each node split, the random forest chooses p features from the m total features of the samples [46, 49]. Among p features, the random forest selects a single feature for a node split based on the "Gini-index" criterion. The Gini-index for each right and left daughter node can be calculated as: $G_r = 1 - \sum_{j=1}^N P_{rj}$ and $G_l = 1 - \sum_{j=1}^N P_{lj}$. Here, P_{rj} (P_{lj}) and N are the probability of the samples in the right (left) nodes having class j and the total number of the classes. The features that maximize the change in the Gini-index that is calculated as follows: $\Delta\theta(s_q) = G_q - \rho_{rq}G_r - \rho_{lq}G_l$ is used for the node split

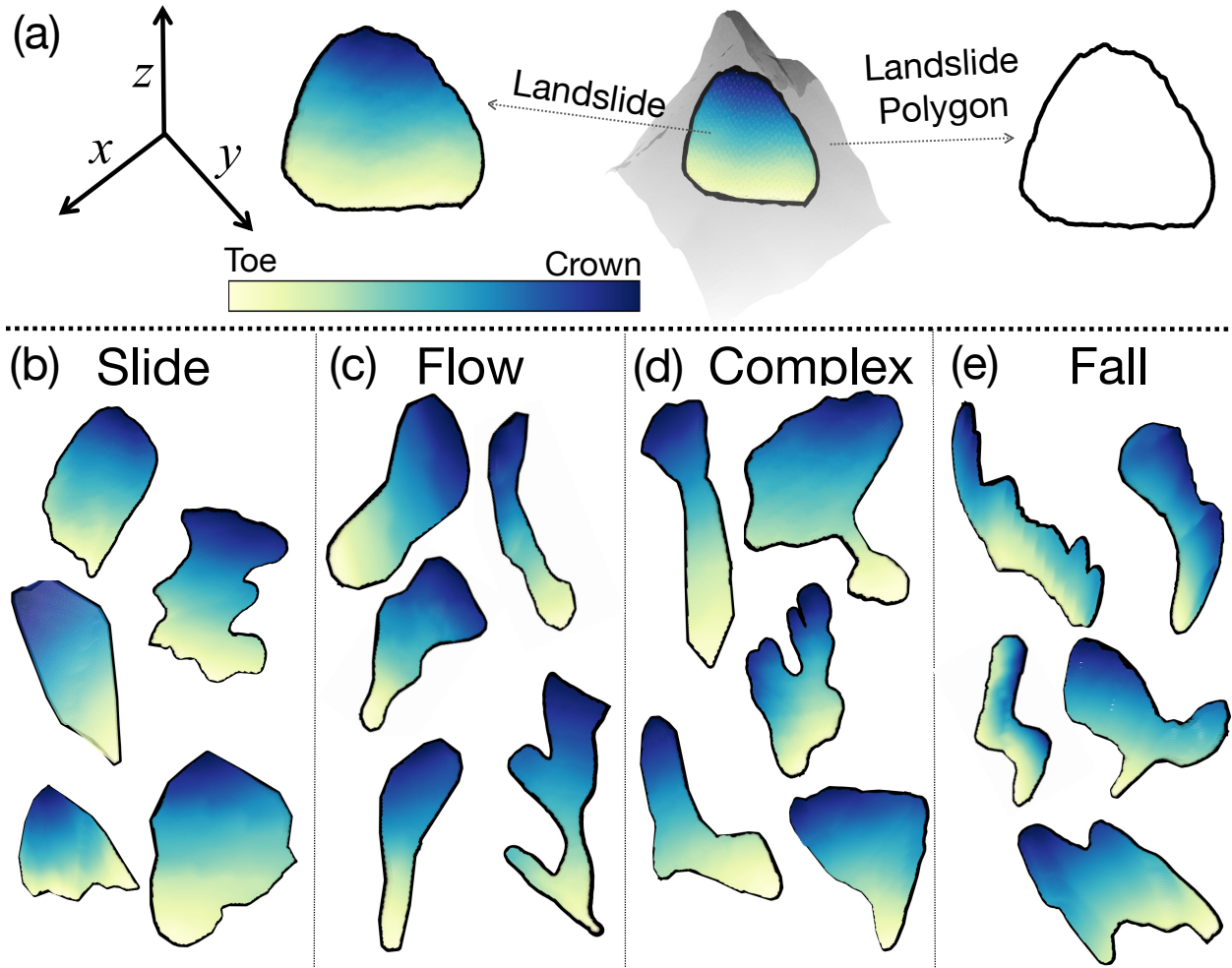


Figure 3: (a) An example of a landslide failure in a terrain with a steep slope. The diagram also shows the 3D landslide polygon, which outlines the landslide shape. (b-e) 3D landslide samples for different landslide failure types, namely, the slide, flow, complex, and fall types.

[50, 51]. Here, ρ_{rq} and ρ_{lq} are the proportion of samples in the right and left daughter nodes. The process of splitting nodes continues until a stopping criterion is met, such as when no more samples are available for splitting, or when the Gini-index of parent nodes is lower than that of daughter nodes.

3 Results

3.1 Landslide topology as a proxy to identify failure types based on style of movement

The underpinning of topological data analysis (TDA) is rooted in structures in the data's shape, such as connected components and holes. Holes represent the empty spaces in the data's shape, and connected components represent the connection of the data's points linked by a continuous path. Using the holes and connected components, we can calculate various topological properties to quantify a shape. For this, we perform the TDA on landslide shapes to compute topological properties which can then be used as a proxy to investigate the underlying failure types. It is important to note that we employ 3D point clouds (containing geographical latitude, longitude, and elevation information) from the landslide's outline (see Figures 3 and 4) obtained via the landslide polygon and the Digital Elevation Model (DEM). The landslide polygon provides the best available approximation of the landslide boundaries in the geographic space, as derived by standard surveying methods with suitable accuracy.

The degree of compactness in a landslide shape is essential when identifying failure types [26]. For instance, slides are characterized by a more cohesive material that tends to remain as a single component (e.g., slides with clay-rich soil

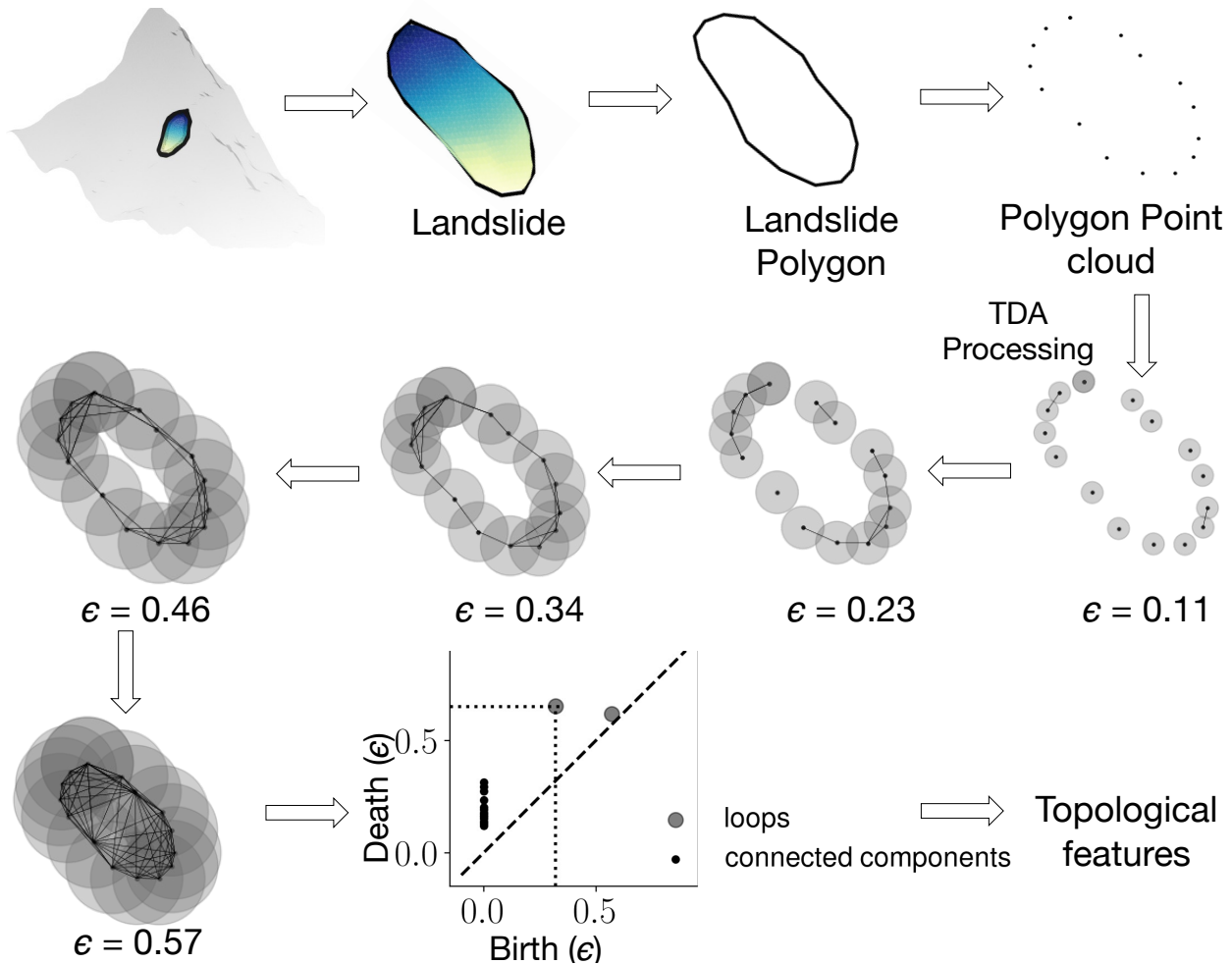


Figure 4: The diagram illustrates the procedure of computing topological features corresponding to a landslide shape. The flowchart shows the use of persistent homology in capturing various structures of the landslide shape by using an evolving disk size (ϵ) around each point in the point cloud. With the increase in ϵ , various structures like connected components and holes emerge in the data's shape which is captured by the persistence diagram. Using this information, we can calculate the topological properties of the landslide's shape. Please note that when processing the TDA features, we display the flowchart using a 2D illustration for simplicity and better visualization.

[52]), leaving behind a more compact-shaped footprint as they fail. In contrast, flow type failures involve more fluid and fragmented materials deposited on a debris fan and display viscous/fluid kinematics that follows the channelized topography of the natural landscape and are less compact. On the other hand, falls consist of fragmented materials that roll/bounce off steep cliffs with a rather shorter and straighter run-out path compared to flows which leave behind a footprint that has an intermediate degree of compactness between the slide and flow-type failures.

We use the amount of empty space inside the footprints of the landslide shape outline to quantify its compactness. To give a simple example, a higher amount of empty space in a landslide shape outline is associated with a higher degree of compactness (e.g., for slide-type failures as seen in Supplementary Figure S1-a). Representing the average lifetime of holes, AL_H (one of the topological properties) computes the hole's average size and estimates the information pertaining to the empty space, and thus the compactness of a landslide's shape. So, landslide shapes with a longer AL_H are more compact than shapes with a shorter AL_H . Based on the Probability Density Function (PDF) of the AL_H , our analysis reveals that slides are more compact than flows, falls, and complex landslides because they have a longer AL_H (see Figure 5). Moreover, we observe the AL_H PDF curve for falls to lie between those of slides and flows, showing that empty spaces generated in falls do not survive long since materials detach from steep slopes and travel a short distance, thereby leaving behind a footprint that represents an intermediate level of compactness. Also, the PDF of the

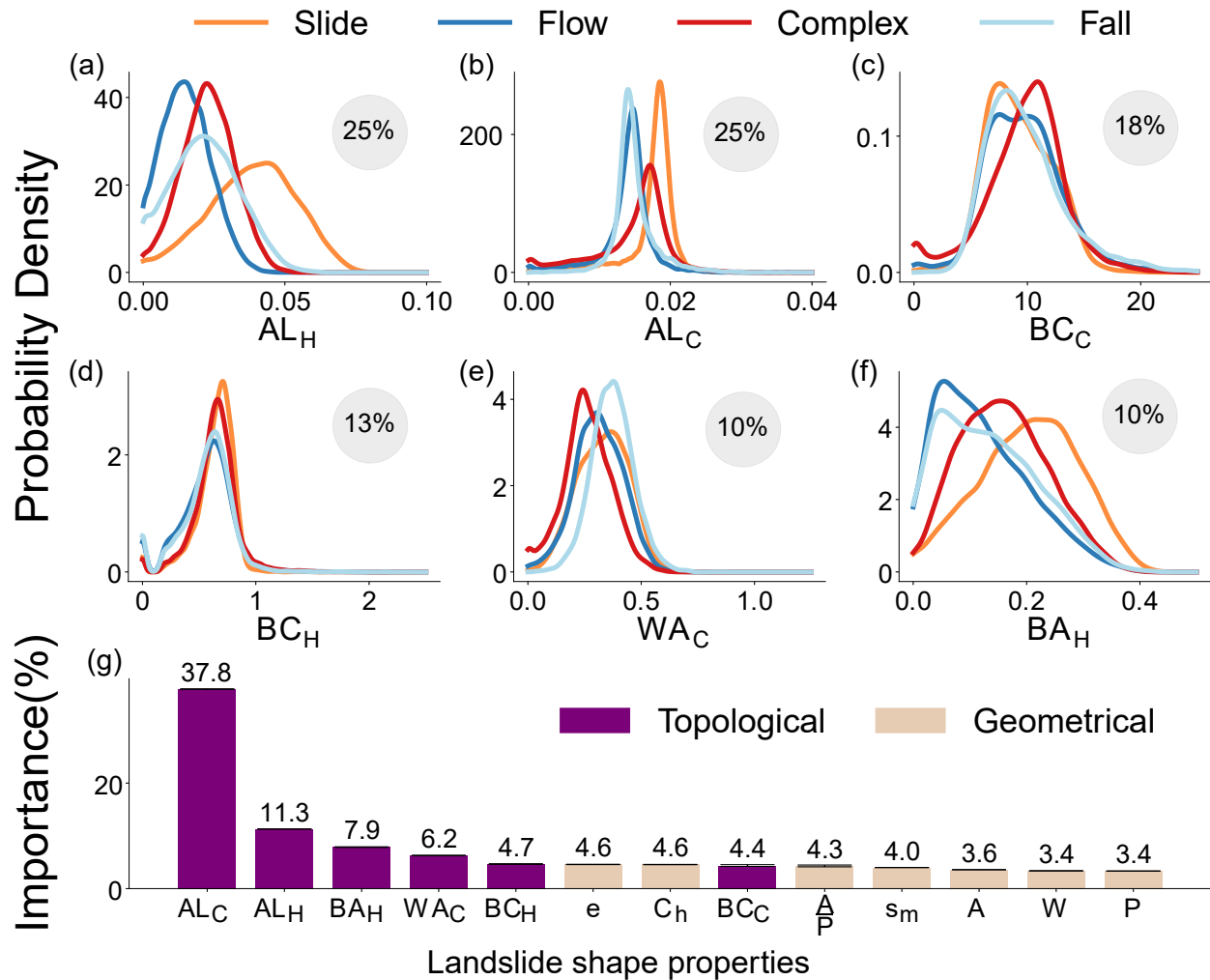


Figure 5: Plots (a-f) show the probability distribution functions of the six most optimal topological properties used in classifying the failure types for slides, flows, complex, and falls in Italy. Please note that we discuss the probability distribution functions of different failure types for the Italian region only, as the Italian data set is the most data-rich inventory. The y-axis shows the probability density values (calculated using kernel density estimation), and the x-axis shows the value of topological attributes. The topological properties in plots (a-f) are: Average lifetime of holes (AL_H), Average lifetime of connected components (AL_C), Betti-curve based feature of connected components (BC_C), Betti-curve based feature of holes (BC_H), Wasserstein amplitude of holes (WA_H), and Bottleneck amplitude of holes (BA_H) (the computations of these properties are explained in detail in Supplementary Section S3 and Figure 4). The percentage values in the gray circular disk in each figure indicate the topological feature's importance (in %), as estimated by the random forest-based classification procedure. Sub-plot (g) shows the joint computed feature importance of topological and geometrical properties by the random forest model. The analysis shows topological properties consistently outperform geometrical properties with a standard deviation under 0.1% (The error bar represents the standard deviation. However, it is not visible in plot-g because the standard deviation is very small). The geometrical properties from top to bottom are: area (A), perimeter (P), the ratio of area to perimeter $\frac{A}{P}$, convex hull-based measure (C_h), minor (s_m), and width (W) of the minimum area bounding box fitted to the polygon.

AL_H for complex landslides shows an intermediate level of compactness, credited to their amalgamated behavior as a combination of slides, falls, and flows.

Another critical property for diagnosing failure types is the sinuosity of the transport zone, which describes the landslide's path or kinematic propagation as it progresses downslope. Among various types of failure, flows exhibit the greatest sinuosity, following the channelized topography more closely than other mass-wasting mechanisms. This is attributed to the fluid and mobile characteristics of the materials involved. In contrast, slides are the least sinuous as

their material is rarely channelized and remains on the open slope, resulting in a relatively straight and uniform path. Fall-type failures are comparatively less sinuous than flows but still exhibit some degree of sinuosity, as they too follow the landscape's topography. Sinuosity defines the existence of numerous curves in the landslide's shape attributed to the landscapes' topography, leading to the generation of partitions within the landslide outlines by the TDA and hence, generating multiple empty spaces with shortened lifetime (see Methods section). This information on the sinuosity of landslide shapes is inferred from the combination of two topological properties—the bottleneck amplitude of holes, BA_H , and the average lifetime of holes, AL_H . The BA_H represents the maximum lifetime of holes in the landslide shape, which quantifies the maximum empty space in the 3D space occupied by the landslide. As sinuous shapes result in numerous smaller empty spaces with shorter lifetimes, the AL_H drops without significantly impacting the largest empty space as determined by the BA_H (see Figure 5). Consequently, a landslide shape with a relatively higher BA_H and a shorter AL_H is indicative of increased sinuosity. In light of these observations, our findings indicate that flow-type landslides indeed display a higher degree of sinuosity compared to other failure types. This is evident from the fact that flows exhibit a similar BA_H to falls but a shorter AL_H in comparison. This is expected, as flows, being the most sinuous, cause multiple small holes or empty spaces (see flow-type and fall-type failures in Supplementary Fig. S1-b,c) that end up shortening the AL_H . Conversely, slides display both longer BA_H and AL_H , reflecting their minimal level of sinuosity.

We are also interested in the role that slope variations play, as they significantly impact the stability of the slope and influence the type of landslide that occurs. For example, falls and slides have a more significant slope transition in their profiles compared to flows, which propagate with a nearly constant slope [53]. This slope variation is captured by the lifetime of the connected components. A sharp change in slope causes the points outlining the landslide to be spaced vertically further apart, leading to a longer lifetime of the connected components. Two topological properties—the Wasserstein amplitude of the connected components, WA_C , and the average lifetime of the connected components, AL_C —help capture information about this slope variation in a landslide's profile. The WA_C quantifies the set of longer lifetimes of the connected components, quantifying the most significant slope change in the landslide outline. This is nicely illustrated in the PDF (Figure 5) of WA_C , which shows that slide and fall failures underwent more drastic slope changes compared to flows. Yet, falls possess a shorter AL_C than slides. This is due to the lower portion of the shape's outline (at the talus) displaying a flatter terrain (representing the area where materials accumulate) and attributing negligible slope change, which ultimately shortens the AL_C . In contrast, flows display the minimum AL_C , as they more or less propagate on constant slopes.

Several topological properties, like the Betti curve-based feature (BC), capture more intricate landslide shape properties and help in discerning landslide failure types. The Betti curve-based feature represents the total number, lifetime, and presence of the structures (holes and connected components) emerging simultaneously. We hypothesize that it encompasses a combination of compactness, sinuosity, slope variations, and similar structures within a given landslide shape. However, the exact connection to the underlying physical types is not clear due to the complex nature of this topological property. We anticipate that such properties consider higher-order information about the landslide shape that is not immediately apparent to us.

Through our analysis, we discovered that common topological properties such as AL_H , AL_C , and BA_C govern the general movements of distinct failure types. These properties act as proxies for the diverse kinematic and mechanical characteristics, which are essential to consider when identifying the different failure types. This finding simplifies and brings coherence to our understanding of landslide behaviors from a topological lens, offering a more effective approach to discerning and predicting these complex natural phenomena.

3.2 Advantages of landslide topology over landslide geometry

Traditional geometric descriptors of landslide shape, including properties such as area, perimeter, and convexity, are derived from 2D representations of the landslide body. As a consequence of this inherent simplification, these 2D-based geometric properties may not adequately capture crucial information, such as failure depth or internal deformations, associated with the landslides' 3D configuration. To address these limitations and provide a more comprehensive understanding of the landslide dynamics, we computed topological properties that are derived from the landslides' 3D configurations. We postulated that the topological properties would prove more meaningful in decoding the characteristics of the landslides and their underlying failure types than the traditional geometric counterparts. To test this, we used a set of seven well-known geometric properties that are commonly employed in the literature [54, 55, 56] along with six topological properties (for the justification of using six topological properties, please refer the Methods section) to determine the failure types in the Italian context.

We jointly computed the feature importance of geometrical and topological properties using the Gini-index feature importance method in the random forest algorithm (see Figure 5-g). After running over 100 iterations on the Italian data set, our findings consistently demonstrated that topological properties exhibited higher feature importance than the traditional geometric counterparts (achieving Micro F1-scores of 94%, ~65% respectively), yielding superior predictive

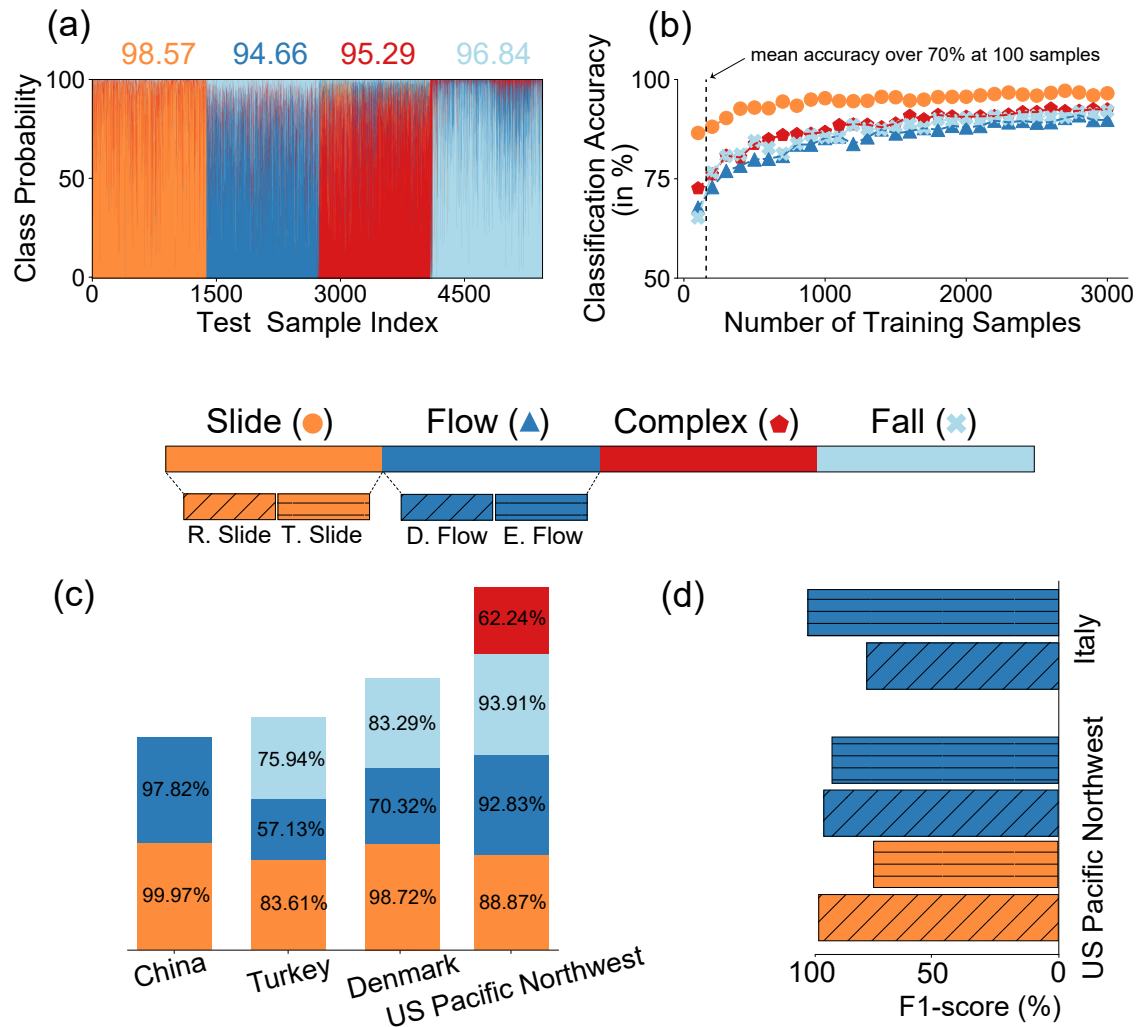


Figure 6: Plot (a) shows the classification accuracy (in %) for each failure class in Italy. The x-axis of the plots shows the testing sample's index, and the y-axis shows the class probability corresponding to each failure class. Plot (b) shows the classification accuracy (in %) corresponding to each failure types with the number of training samples. The x-axis shows the number of training samples from each class used to train the model, and the y-axis shows the classification accuracy (in %) corresponding to each class. At 100 samples, the mean classification accuracy already reaches over 70% in Italy. Plot (c) demonstrates the model's versatility in accurately identifying various types of landslides across multiple geographical regions, including China, Turkey, Denmark, and the US Pacific Northwest, with their corresponding F1-scores listed for each type. Plot (d) highlights the model's capability to distinguish sub-types of landslide failures specifically in the US Pacific Northwest and Italy. In the US Pacific Northwest, the model successfully classifies four additional sub-types—rotational slide, translational slide, debris flow, and earth flow—with an average F1-score of 84% along with the other failure type classes (complex and fall type). In Italy, the model identifies two additional sub-types—debris flows and earth flows—with an average F1-score of 96% along with the other failure type classes (slide, complex, and fall type).

capabilities for identifying failure types. Additionally, we observed that even the least important topological property (BC_C) has similar feature importance as the other geometric ones, while the former conveys unique information about the landslide shapes as discussed in the previous section. Moreover, we calculated the Probability Density Function (PDF) for both geometric and topological properties and observed that the latter had greater dissimilarity than the former among different failure types (see Supplementary Figure S2). These two findings demonstrate that topological properties are stronger predictors for identifying failure types. The reason for this can be attributed to the enhanced capacity of topological properties to encapsulate important information pertaining to landslide kinematic progression, failure depth, sinuosity, compactness, and slope variation.

3.3 Determining failure types with TDA and machine learning

Next, we employed Topological Data Analysis (TDA) to compute a diverse array of topological properties/features using the landslide inventory of Italy. Subsequently, we conducted a correlation analysis and feature importance assessment to identify the six most optimal properties out of thirty. Our evaluation unveiled that several TDA properties were redundant, amplifying the model's complexity and undermining its predictive potential. Consequently, we opted to eliminate the irrelevant ones. Leveraging the six best features, we applied the random forest algorithm to discern the failure types. We independently scrutinized the performance of our approach using various training and testing sets for the Italian inventory.

We applied the model to approximately 250,000 landslide samples, ensuring balanced training by using an equal number of samples—13,000 for each landslide type. To mitigate overfitting and bias, we performed 10-fold cross-validation 1,000 times on a subset of 54,440 samples. This approach yielded a Micro F1-score, a key performance metric, surpassing 94% for each failure type (see Figure 6-a), with a performance standard deviation of less than 0.2%. This illustrated the robustness of our methodology in handling variations among training samples across Italy. We examined various other metrics (Supplementary Figure S3), such as the True Positive Rate (TPR) and True Negative Rate (TNR), to evaluate the method's performance. These metrics consistently exhibited high scores across all classes, thereby ascertaining the model's classification ability.

3.4 Method transferability to different regions of the world

In this sub-section, we assess the performance of our method's transferability across both historical and event-based landslide inventories that include spatial and temporal data. Additionally, we tested the method's efficacy in scenarios where information on failure types is either scarce or lacking. To evaluate the method transferability in diverse geomorphologies and climatic regions, we deploy the method in the Pacific Northwest of the US (states of Oregon and Washington), Denmark (national inventory mapped by Luetzenburg et al.[57]), Wenchuan (China) inventory mapped by Fan et al.[58] for the 2008 earthquake event, and Turkey (municipality of Ulus) mapped by Gorum et al.[59]. The method achieved above 80% mean classification accuracy in each region in identifying failure types (see Figure 6-c).

Moreover, we implemented the method in an event-specific inventories from the multi-temporal inventory from Wenchuan, China containing eight event-specific inventories from distinct years, triggered by a combination of rainfall and earthquakes. To assess the method's performance on an event-specific inventory, we trained the model using one of the earthquake-triggered inventories from 2008 and then tested it on the remaining inventories from the subsequent years (2011 to 2018). Across all the testing inventories, our method achieved a mean classification accuracy of over 90% (see Figure 7-c). Additionally, we implemented the method on two undocumented inventories predating the 2008 event, specifically from the years 2005 and 2007. In our prediction of the landslide types within these inventories, we found that most were identified as debris flows (119 in 2005 and 40 in 2007), with the remaining few classified as debris slides (13 in 2005 and 32 in 2007). We manually verified the method's predictions for these landslides using ArcGIS and Google Earth archive imagery (see Figure 7-a, b).

To assess our method's performance in regions with limited documented failure-type samples, we conducted an experiment with a decreasing number of training samples. We discovered that with just 100 samples from each class, our method achieved a mean classification accuracy exceeding 70% using the Italian dataset (see Figure 6-b). This highlights our approach's capability to operate effectively in regions where failure-type samples are scarce. For areas entirely lacking documented failure information, the model can be used by manually annotating a modest set of around 100 samples. This provides a practical solution for a streamlined, automated failure type classification system for documenting failure types in large landslide databases, often containing thousands of entries.

3.5 Determining sub-type failure movements of the landslides

Sub-type classification of landslides is critical for devising targeted mitigation strategies and understanding the underlying mechanics that drive these failures. To address this need, we go beyond the general categorization of landslide failure types to test the ability of the model to identify/classify specific landslide typologies for the inventories of Italy and the Pacific Northwest of the USA. In the case of Italy, we tested with five sub-type failure movements ('Slides', 'Debris flows', 'Earth flows', 'Complex landslides', and 'Rock falls') achieving an F1 accuracy of 96% while in the case of the Pacific Northwest of the US, we tested with six sub-type failures ('Debris flows', 'Earth flows', 'Rotational slides', 'Translational slides', 'Rock falls', and 'Complex landslides') achieving an average F1 accuracy of 84% (see Figure 6-d). This extension demonstrates that our method can handle more than the basic four classes or types, including differentiating sub-types within slides (such as rotational and translational) and flows (including earth flow and debris flow). Such distinctions are vital for type-specific predictive modeling and a comprehensive understanding of landslide movements, as well as the underlying causes of their behaviors. This success can be attributed to the TDA's

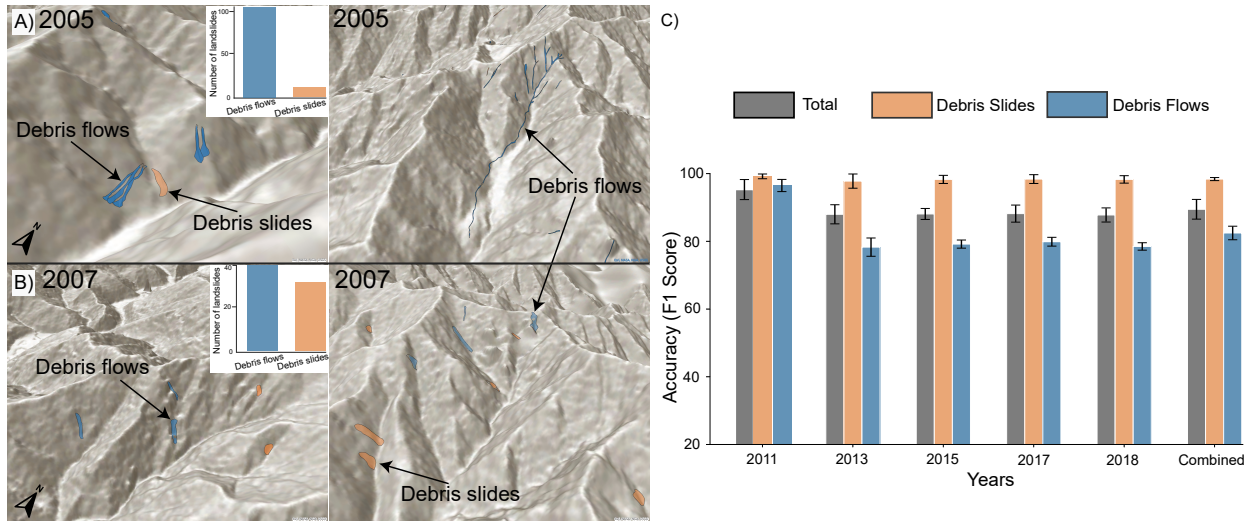


Figure 7: Rows (a) and (b) display snippets of proposed method predictions in two undocumented databases from the 2005 and 2007 inventories of Wenchuan, China, respectively. Each row in these plots shows debris slides and flows as identified by the model, with the accompanying bar chart quantifying the number of landslides by their type. Plot (c) shows the method performance on multi-temporal databases triggered by either earthquake or rainfall spanning from 2011 to 2018 years. The model is trained on the 2008 inventory associated with that year's co-seismic event for each testing year. The chart also includes a composite dataset derived from combining all these multi-temporal inventories. Error bars in the chart indicate the standard deviation for each landslide type within each inventory. The model achieved an average F1-score of 89%, with an average standard deviation (for the F1-score) of 4%. The base map was sourced from the World Hillshade Map. Map credits: World Shaded Relief-ESRI[32].

capability of discriminating among various failure types like debris flow and earth flows. This differentiation arises from the inherent morphological variations between debris (characterized by more sinuous and longer trails) and earth flows (marked by less sinuous and relatively shorter trails).

3.6 Identifying failure types within the complex landslides

Complex landslides typically occur as amalgamations of numerous processes or failure types that appear successively, such as slides to flows [60]. Because complex landslides include multiple failures, it is challenging to investigate their behavior for the purposes of predictive modeling. Topological properties are capable of capturing intricate information between different failure processes (as seen in the previous sections), and hence, we further explored its capability to understand the underlying coupled failure types that form complex landslides. We utilize 428 complex landslides from the US Pacific Northwest data set to discern the combination of failure types present in them. Out of 428 complex landslides, 198 of them are documented as "Translational rock slides followed by rock falls" and the rest are documented as "Rotational slides followed by flows" (as reported by the Statewide Landslide Information Database for Oregon, SLIDO [61]).

To identify the failure types within these complex failures, we trained our method with three classes (i.e., slides, flows, and falls) and forced the model to predict the class probability corresponding to each failure type. For 198 complex landslides documented as "Translational rock slides followed by rock falls", our model predicts slide-type failures with the highest probability followed by falls (see Supplementary Figure S4-d). Similarly, for the remaining 230 "Rotational slides followed by flows" complex landslides, our model predicts slide-type failures with the highest probability followed by flows (see Supplementary Figure S4-e). Among these 428 landslides, sliding failures are predicted as the most dominant failure type, which is also evident when observing the resemblance of the slide and complex failure topological properties (such as AL_H , BC_H , and BA_H) in the PDF plots (see Supplementary Figure S4-a,b,c). These findings demonstrate that topological properties are able to capture more than just one physical process in a given landslide and that they could be used to automatically improve large Varnes-based inventories toward Cruden and Varnes-based classification.

4 Discussions

In this work, we attempt to determine the failure types based on their movements through the lens of landslide topology. Our key findings elucidate the connection between the topological properties as a proxy to identify underlying failure movements. We observe that identical landslide types harbor similar topological properties, indicating the presence of common morphological characteristics that govern the general movement of the failures. We find that topological properties offer a more profound capacity to distinguish between failure types than traditional geometric properties (please see result sub-section on landslide topology as a proxy to identify failure movements). This finding can be attributed to the fact that topological properties inherently capture critical information related to landslide kinematic progression, failure depth, sinuosity, compactness, and variations in slope. In contrast, geometric properties tend to oversimplify the complex spatial, kinematic, and mechanical relationships that govern the behavior of landslides and are hence less effective in differentiating between various failure types. Building on the advantages of topology over geometry, we developed a method using the Italian landslide inventory that utilizes topology to identify failure types.

The next valuable step involved recognizing our method's capability to adapt across diverse geomorphological and climatic settings, including both historical (such as Italy, the US Pacific Northwest, Denmark, and Turkey) and event-based inventories (such as Wenchuan, China). This exploration yielded noteworthy results, as our method is capable of identifying failure types across these varied regions. This opens up opportunities for transferability and provides a path toward identifying failure movements in previously undocumented inventories. Consequently, recent events and their corresponding inventories would benefit from this approach, as they could be efficiently classified by employing our method.

Beyond providing a transferable method, our approach also opens new possibilities for studying the complexity and evolution of landslide behavior, with the potential to improve hazard forecasting [54]. As demonstrated in the temporal experiment of Wenchuan, China, our approach admittedly holds the ability to identify failure movements across not just space but also time, with which we were able to also recognize and quantify the failure movements in two undocumented inventories predating the Wenchuan earthquake event (Mw 7.9) of 2008 (please see the transferability results sub-section). Such information carries substantial importance as it paves the way for focused research into quantifying (re-)mobilization of failures, extracting precise data on sediment budgets, and understanding dominant geophysical cycles at continental and global levels [62, 63, 64, 65].

Drawing on the experiments of the sub-type classification (for e.g., debris and earth flows) of landslide failures using the Italian and the US Pacific Northwest dataset (please see the sub-type results sub-section), we recognize the substantial value in identifying and quantifying these sub-movements, bearing notable potential to enhance both landslide risk assessment and related hazard models [20]. The level of damage to infrastructures and the risk of human casualties vary depending on the intensity of the failure movement, which differs for each failure type [14]. For example, a slow-moving deep-seated rotational landslide (1.5 m/year to 16 mm/year) may not pose an immediate threat to the population, but it can cause extensive structural damage to buildings over a prolonged period [66, 67]. In contrast, flow-type failures, such as debris flows, have rapid mobility and can result in significant casualties and infrastructure damage simultaneously [68, 69]. Similarly, episodic impacts in fall-type failures can cause massive damage to infrastructures in a matter of seconds due to their high energy (e.g., impact pressure measured in kilopascals, kPa) [70]. We can infer from these broad examples that the availability of failure-type, especially sub-type information could considerably enhance the accuracy of predictive modeling and that incorporating it benefits the landslide community as it enables the development of accurate landslide predictive models.

In addition, we utilized topological properties to dive deeper into complex landslides and identify the underlying coupling of failure types that contribute to their formation (please see "Identifying failure types within the complex landslides" Results sub-section). Our findings in the US Pacific Northwest suggest that topological properties can reveal more than one physical process in a given landscape (for example, identifying coupled failures of slides following falls or slides following flows). This has significant implications for understanding complex landslide failures, which often arise from a combination of different failure movements, such as sliding, flowing, and falling, and may not be fully encompassed by current characterization and classification methods for large-scale analysis. Traditional approaches may struggle to pinpoint the exact cause, leading to hindrances in prevention efforts. The use of topological properties to uncover these intricacies offers a path towards a more comprehensive characterization, where capturing the dominant failure type would enable pinpointing the possible initial failure within the complex landslide. Given these advantages, we anticipate that our method will open new avenues for future research, particularly in the landslide modeling community, for example, working on large-scale post-event mapping and large- to medium-scale hazard forecasting.

While the proposed solution demonstrates notable success in identifying failure types, there are inherent limitations that warrant attention. The effectiveness of the method relies on the quality and geographical location of the training

and testing data used in the model. Manual annotations of failure types can lead to bias since various mappers will have different perspectives (mapping on aerial or satellite imagery versus geomorphological field mapping can display distinct perceptions) when annotating the landslides and their failure types. Also, due to the ambiguous nature of complex-type failures, they could include slides and flows simultaneously, which can impact the overall performance of the model. The method's reliance on a DEM for converting 2D polygons into 3D shapes also presents potential challenges. DEM quality in the training and testing regions can bias the results, particularly for smaller landslides, as coarser DEM resolutions may struggle to capture the profiles of these smaller-scale events.

The potential of the proposed method reaches beyond just understanding the complex interplay between landforms, their shapes, and the underlying geophysical processes responsible for their formation; they also serve as a subject captivating interest across various geophysical disciplines. The ability to acquire knowledge about the processes generating complex landforms based solely on their shapes suggests a rich presence of signatures imprinted on the landscapes. Our method leverages their topological properties to effectively extract this information. Envisioning compelling applications beyond landslides, we can explore other geophysical processes such as permafrost-borne retrogressive thaw slumps in Arctic regions [71] and sub-surface processes, e.g., submarine landslides [72], which commonly occur in a typical data-scarce environment such as the sea bottom, where geological and geotechnical information are almost absent. These processes also give rise to unique landforms displaying distinct shapes and configurations, and employing topology can aid in gauging the mechanisms governing their occurrences. By doing so, our method could shed new light on mathematical and physical phenomena underlying various geophysical and environmental scenarios.

5 Data availability

The dataset we utilized in this study to classify the failure types of landslides was obtained from the *Inventario dei Fenomeni Franosi* (Inventory of Landslide Phenomena) in Italy (IFFI) [73]. The IFFI project catalog (www.progettoiffi.isprambiente.it) was created in 1999, with the aim of mapping and identifying landslides in Italy, and holds information on over 250,000 usable landslide polygons. Aerial image interpretation, historical sources, and field surveys were used to acquire and validate this catalog, while the classification protocol/scheme referred to that of Varnes (1978) [14] and Cruden and Varnes (1996) [74]. In our work, we chose the polygonal landslide data from this catalog and also carried out post-processing to correspond to the spatial extent and resolution of the 25-meter EU-DEM [75].

The study area is the Pacific Northwest region of the United States. The data set from the US Pacific Northwest consists of inventories from Oregon's Statewide Landslide Information Database for Oregon (SLIDO-4.4 updated 10/29/2021; Franczyk et al.[61]), mapped by the Oregon Department of Geology and Mineral Industries (DOGAMI), and the Washington State Landslide Inventory Database (WASLID updated 2018/08/01; Slaughter et al.[76]), mapped by the Department of Natural Resources, Washington Geological Survey (WGS). The combined inventories comprise 47,653 landslides from the US Pacific Northwest region. The inventories contain LiDAR-derived landslide polygons guided by protocol to capture the movement types with spatial information on the scarps, head scarps, toes, and deposits [77, 78, 76]. Since this data is categorized using a combination of Cruden and Varnes [74] and Hungr et al. [13] (i.e., slides, flows, complex, and falls), we modified the Italian data correspondingly to maintain uniformity in the taxonomy of the failure mechanisms.

The national landslide inventory of Denmark was obtained from Luetzenburg et al.[57], published in 2022. The landslides were mapped via high-resolution DEM of 2015 and orthophotos supplied by the Danish Agency for Data Supply and Infrastructure, consisting of 3202 unique polygons of mapped landslides following the classification from Hungr et al.[13].

The landslide inventory of Turkey was obtained from Gorum[59] published in 2019. The landslides were mapped from airborne LiDAR data with a total count of 900 landslides classified according to the Cruden and Varnes[79] system.

Landslide inventory of the Wenchuan region of China was acquired from Fan et al.[58] where they generated a multi-temporal inventory of the infamous Wenchuan 2008 earthquake event causing thousands of landslides. The multi-temporal window spans from 2005 to 2018, mapped with a custom classification system based upon a simplification of the Hungr et al.[13].

The EU-DEM for Italy and Denmark was downloaded from <https://land.copernicus.eu/imagery-in-situ/eu-dem/eu-dem-v1.1> and the DEM for the US Pacific Northwest was downloaded from <https://www.opentopography.org/>. The Shuttle Radar Topography Mission (SRTM) DEM for China and Turkey was downloaded from <https://dwtkns.com/srtm30m/>

Code availability

Data analysis and processing were conducted using Python programming language and its associated libraries. The various scripts used for data analysis are available at <https://github.com/kushanavbhuyan/Uncovering-landslide-failure-types>.

Author Contributions

KR, KB, UO, and NM contributed to the conceptualization and design of the research. JVF and KB curated the data. KR and KB developed the methodology and conducted the formal analysis under the close supervision of UO, FCo, FCo, and NM. All authors contributed to writing, review and editing.

Acknowledgments

We extend our gratitude to Dr. Tolga Gorum and Dr. Hakan Tanyas for providing access to the Türkiye landslide inventory dataset, which served as an essential resource for empirically evaluating the model's transferability.

Competing interests

The authors declare no competing interests.

Supplementary Materials: Landslide Topology Uncovers Failure Movements

S1 Introduction

This supporting information (SI) to the manuscript titled “Landslide topology uncovers failure movements” includes a detailed analysis of landslide topology and its importance in finding the landslide failure types based on their movement. The SI includes an in-depth analysis of the topological features and their probability distributions, quantifying the differences among the different failure types and the connection between the landslide topology and the physical processes. Moreover, we include a section for a detailed evaluation of the model and its transferability analysis. We also show that landslide topological information provides more information about landslide shape than classical geometric information like area, perimeter, and ellipticity, and therefore can be helpful in other landslide research.

S2 Behavior of different failure types

The inherent differences between failure types, notably their kinematic and mechanical behaviors, contribute prominent intricacies to the topography (see surface profiles in Figure 1 in the main manuscript). These intricacies are attributed to slope deformity, interior deformation, kinematic width of failures while propagating down-slope, main scarp deformation, run-out length represented by the debris/earth/soil transportation, and accumulated debris, and others captured by topology. The following are some of the most common failure types and their various behaviors.

The profile of rotational slides is marked by a conspicuous primary scarp and a distinctive back-tilted bench at the head, but little interior deformation (a schematic view can be seen in Figure 1 in the main manuscript). They are typically slowly moving a large portion of the weak rock mass. At the same time, kinematically rapid planar sliding is marked by the sliding of a rock mass on a planar rupture surface with little to no internal deformation, where the scarp might be separated from the stable rock at deep vertical tension cracks. Typically, they exhibit very compact shapes. Cohesion, c plays an important role in slides, as the degree of internal strength between the particles in a block of material determines the strength and stability along the slip plane. Translational landslides, like the ancient Seimareh slide in Iran’s Zagros Mountains, are among the largest and most destructive on Earth [80].

Flows are characterized by very rapid movements consisting of saturated granular material on moderate slopes, including liquefaction of materials (in the context of co-seismic triggers) or excess pore pressure (in the context of rainfall triggers) originating from the landslide source. When the internal friction angle, φ , is low (due to the mixture of solid and fluid particles), less external force is required to instantiate a failure because they are displaced quite easily. Kinematically flow-ish movements are observed with channelized streams and a bulk deposit of debris at the talus (deposition zone), representing highly elliptical, elongated bodies [81].

Usually limited in volume, falls (particularly rock falls) exhibit ballistic movements (high velocity, energy, and momentum) that are massively destructive. They detach from cliffs and move at high velocities, either by rolling, falling, or bouncing due to the influence of gravity. The run-out of a rock fall is often shorter and is more likely to travel along a straight path, whereas the run-out of debris flows is longer and can meander and spread out over a wider area [16].

Complex failures are very hard to describe, as there is an amalgamation of different failure types occurring at the same time or subsequently, and they can therefore exhibit multiple characteristics of other failure types. For example, irregular debris slides evolving into a debris flow or any other combination of slides, flows, and falls eventually evolving into another movement style can be considered examples of complex failure [74, 13].

Such morphological and geometrical information for each distinct failure type is theorized to be captured in the topological space by the topological properties, which are then utilized in the machine-learning model to identify the failure types.

S3 Topological Features

Persistence diagrams capture the life-death information of structures like connected components, holes, and voids. The persistence diagram consists of a set of $\{(b_i, d_i)\}_{i=1}^{i=N}$ pairs corresponding to each structure type; here, i and N are the indexes of birth-death pairs and the total number of the birth-death pairs. Using the set of $\{(b_i, d_i)\}_{i=1}^{i=N}$ pairs, we can calculate various topological features such as persistence entropy, average lifetime, number of points, Betti curve-based measure, persistence landscape curve-based measure, Wasserstein amplitude, Bottleneck amplitude, Heat kernel-based measure, and landscape image-based measure.

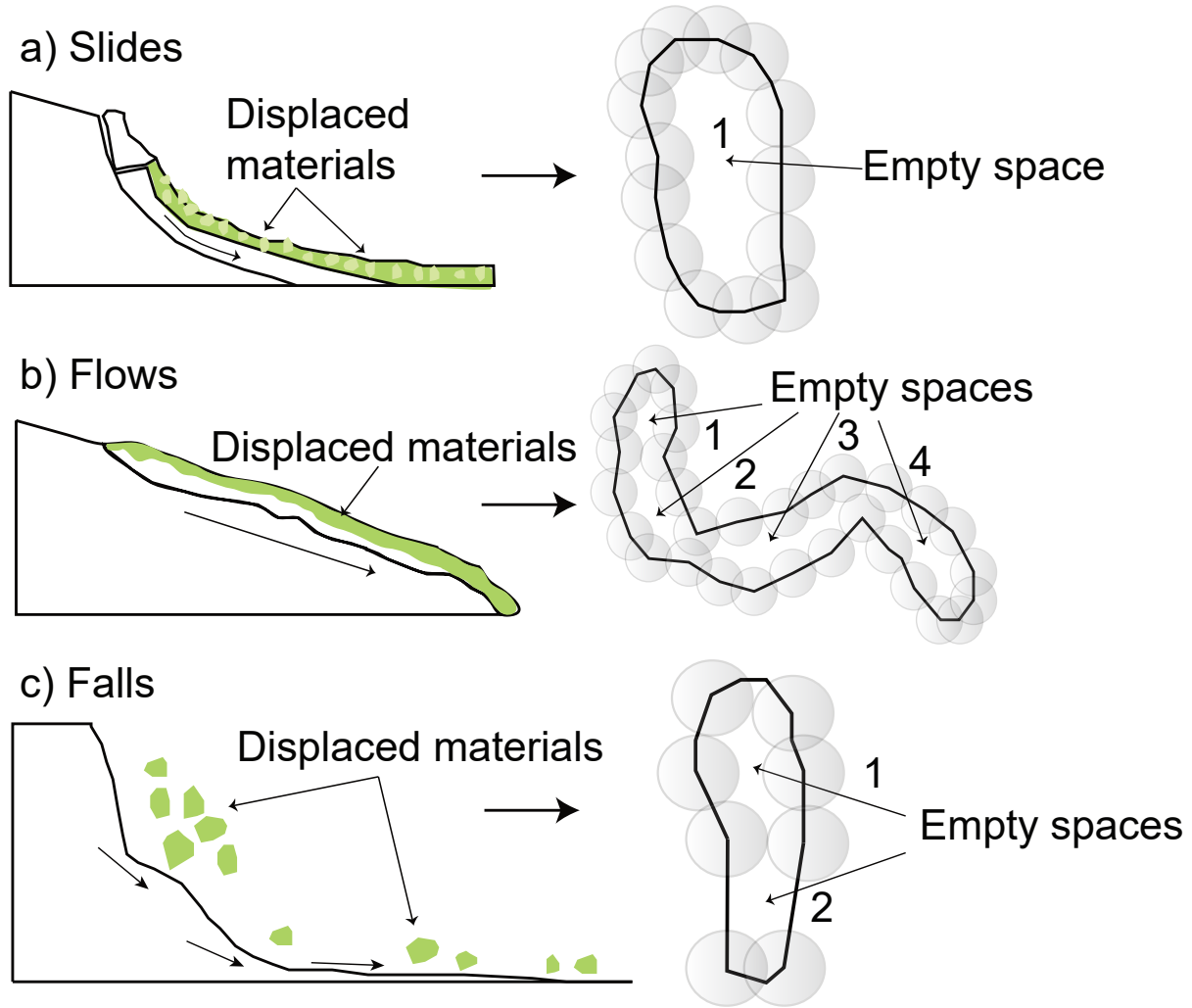


Figure S1: The diagram shows a schematic outlook of how empty spaces are created in different landslide types. This illustration is shown using a simplified 2D transformation of a rather complex 3D topological phenomenon for ease of understanding. Sub-plots (a–c) refer to the possible configurations of empty spaces created in the typical polygons of each failure type. Slides tend to have the fewest empty spaces or holes due to their compact shapes, followed by falls. Flow-type failures tend to have multiple numbers of empty spaces due to the sinuous shapes they conjure as they follow the landscape’s channelized topography.

Some of the above topological features can be explained using a lifetime vector that is calculated using a set of $\{(b_i, d_i)\}_{i=1}^{i=N}$ pairs. The lifetime vector $[l_i]_{i=1}^{i=N}$ is calculated as the difference between death and life of the (b_i, d_i) pair ($l_i = d_i - b_i$). The number of points, average lifetime, and persistence entropy are the length, average, and Shannon entropy of the lifetime vector. In comparison, topological features like Bottleneck and Wasserstein’s amplitudes quantifying the magnitude of the lifetime vector are p -norm ($p=2$) and ∞ -norm of the lifetime vector, respectively.

The Betti curve-based feature is a p -norm of a 1D discretized betti curve, which is a function $(B(\epsilon) : \mathbb{R} \rightarrow \mathbb{Z})$ mapping the persistence diagram to an integer-valued curve, and it counts the number of birth-death pairs at a given ϵ , satisfying the condition $b_i < \epsilon < d_i$ [36]. Similarly, a persistence landscape curve-based feature is a p -norm of a 1D discretized persistence landscape curve defined as $\lambda(k, \epsilon) : \mathbb{R} \rightarrow \mathbb{R}_+$, where $\lambda(k, \epsilon) = k_{max}\{f_{b_i, d_i}(\epsilon)\}_{i=1}^{i=n}$, k_{max} is the k -th largest value of a set of functions defined by $f_{b_i, d_i}(\epsilon) = \max\{0, \min(\epsilon - b_i, d_i - \epsilon)\}$ for each (b_i, d_i) pair [38].

The heat kernel-based feature is a p -norm ($p=2$) of the discretized 2D function obtained using the operation of the heat kernel on the persistence diagram. Heat kernel uses a gaussian kernel (σ) and a negative of the gaussian kernel (σ) for each (b_i, d_i) pair and mirror of (b_i, d_i) pair across the diagonal [39]. In contrast, the persistence image-based feature

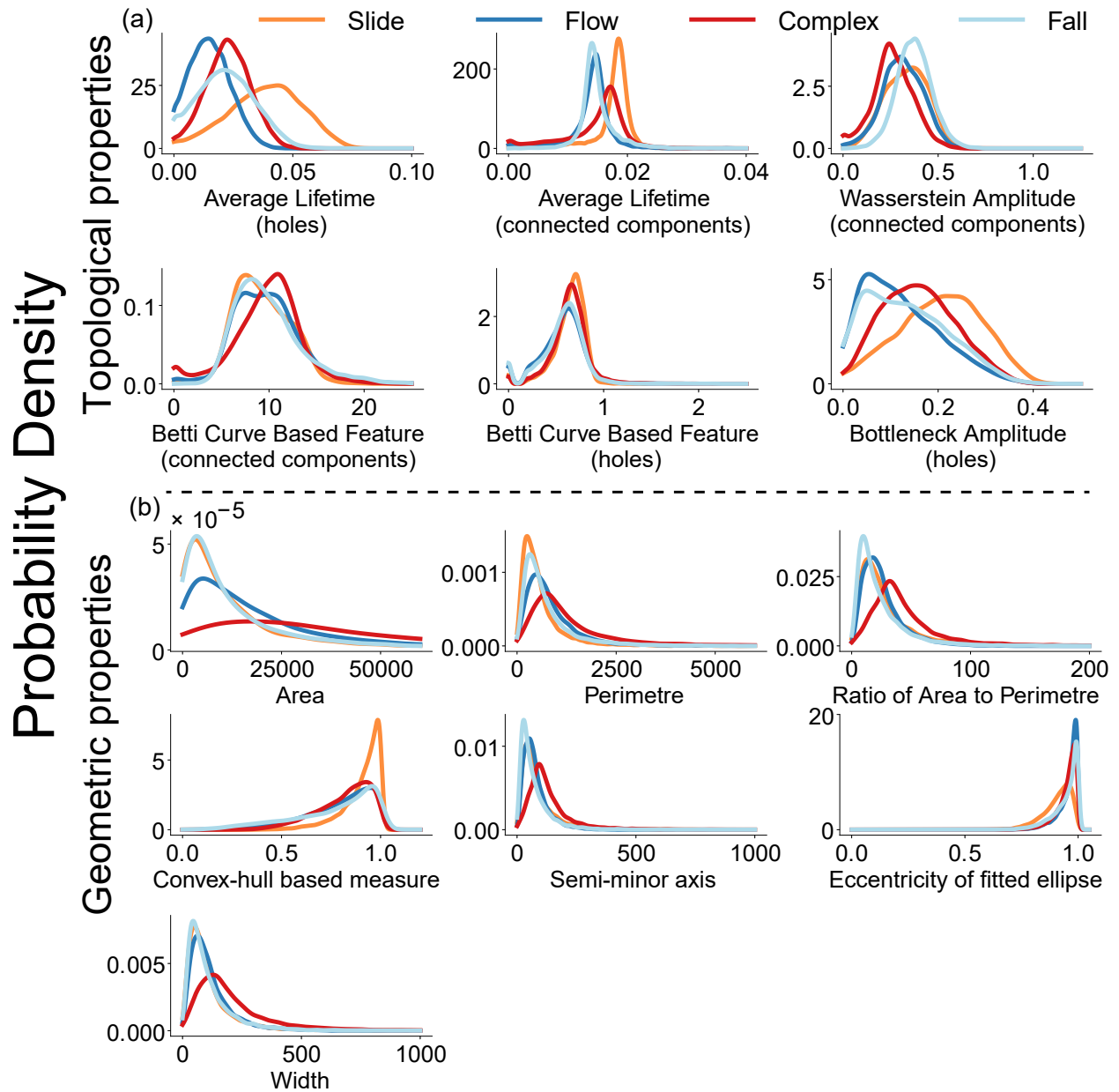


Figure S2: Probability distribution functions of the geometrical and the topological features for each failure type– slides, flows, complex, and falls–in Italy. The y-axis shows the probability density values (calculated using kernel density estimation), and the x-axis shows the value of topological or geometrical attributes. The geometric features from top to bottom are: area (A), perimeter (P), the ratio of area to perimeter $\frac{A}{P}$, convex hull-based measure (C_h), minor (s_m), and width (W) of the minimum area bounding box fitted to the polygon.

is a p-norm ($p=2$) of the discretized 2D function obtained using the operation of the weighted Gaussian kernel on all $(b_i, d_i - b_i)$ pairs in the birth-persistence diagram [40]. The birth-persistence diagram consists of $(b_i, d_i - b_i)$ pairs where the x-axis shows the birth information, and the y-axis shows the lifetime of the (b_i, d_i) pair.

		Predicted Class			
		Slide	Flow	Complex	Fall
Actual Class	Slide	98.60	0.00	1.18	0.22
	Flow	0.0	94.77	1.70	3.53
	Complex	0.66	1.99	96.39	0.96
	Fall	0.15	2.80	0.96	96.11

	Slide	Flow	Complex	Fall
TPR	98.50	94.69	96.27	96.00
TNR	99.69	98.38	98.67	98.40
FPR	0.30	1.61	1.32	1.59
FNR	1.49	5.30	3.73	3.97
F1-Score	98.79	94.90	96.16	95.64

Figure S3: The figure shows the confusion matrix and the associated accuracy metrics of the random forest model for the data of Italy.

S4 Geometric versus Topological Features

Geometric properties define an object’s shape and size, but topological properties explain the connections and topological interactions among its parts. Geometric properties such as area, perimeter, convexity, and ellipticity define the physical dimensions of a landslide, whereas topological properties such as the average lifetime of holes, Betti curve, and landscape curve describe the connections and interactions of the soil and rock masses, the width of kinematic propagation, and depth of failure in a landslide. Geometric properties are, however, sensitive to any changes made to the original shapes of the geometry and therefore, more susceptible to drastically changing the geometric property values. For example, any change to a landslide’s boundary/body would inadvertently change each of the values of the geometric properties like area, perimeter, convexity, etc., but the same cannot be said for topology as it relies on the number of voids that are generated based on the overall shape of the landslide body. This is even more pronounced upon investigating the landslides in 3D. Since these geometric properties cannot be broadcasted to 3D, much information related to variational changes in the topography (attributed to elevation and slope) is lost. As TDA captures this 3D information and utilizes it when engineering topological features, intricate information on landslides such as depth of failure, deformations pattern, and the width of kinematic progression are well recorded.

Therefore, to assess and evaluate the differences between the classical and topological properties, we compare them in this section. This comparison was based on KDE plots that represent the PDFs of the samples for each failure type. We also plotted box plots to compare the median values and distribution of said values between the geometric and topological properties. As we see in Figure S2-b, the PDFs of the failure types are very similar to each other, specifically when looking at the ellipticity, semi-major axis, perimeter, and width. However, when comparing them to

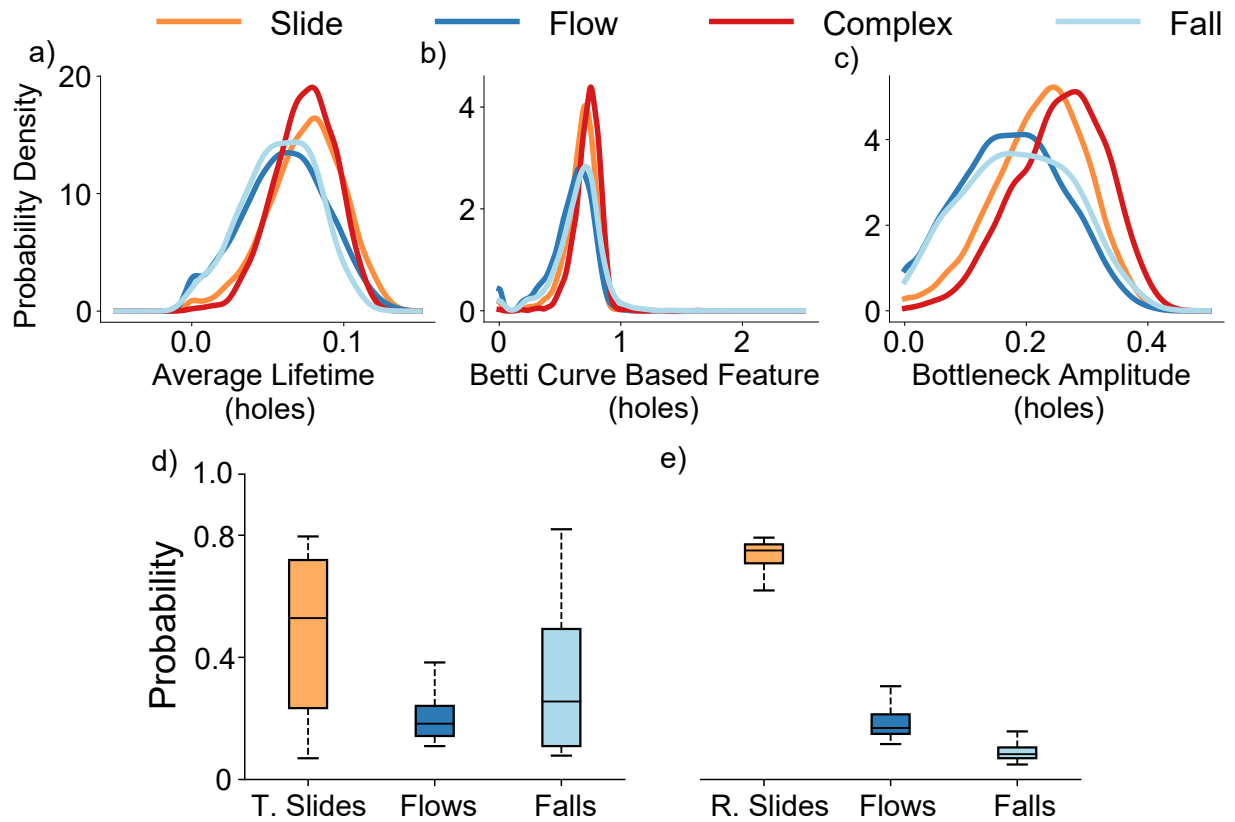


Figure S4: Sub-plots (a-c) display the probability distribution functions for three key topological properties for the US Pacific Northwest: Average Lifetime of holes, Betti curve-based features of holes, and Bottleneck amplitude of holes. These distributions reveal a striking similarity between sliding-type and complex landslide failures. Sub-plots (d-e) show the probability of complex landslides belonging to each of the failure types class (slide, flow, and fall) as predicted by the model. Box plot (d) shows the complex landslide samples that occur from "Translational rock slides followed by rock falls" as documented in the Statewide Landslide Information Database for Oregon (SLIDO). Model predictions indicate sliding failure to be the predominant type of failure, which are most likely translational slides according to SLIDO. Similarly, box plot (e) shows the complex landslide samples that occur from "Rotational slides followed by flows" as recorded in SLIDO. Model predictions indicate slide type to be the predominant type of failure, which most likely ruptures rotationally. Beige bars illustrate sliding mechanisms while bars with darker and lighter shades of blue illustrate flows and fall types, respectively. Note the number of annotated complex failures with behavioral definitions by SLIDO in box plot (a) constitutes 198 samples and box plot (b) constitutes 230 samples.

the topological properties Figure S2-a, we observe that the PDFs of the failure types are more dissimilar to each other under each property (e.g., the average lifetime of holes, bottleneck amplitude of holes, Wasserstein amplitude of holes). This can be the reason why the random forest models show promising results, as the PDFs are dissimilar enough to find evident differences between each failure type when using the topological properties/features.

S5 Other measures to evaluate model performance

In order to evaluate the performance of the method, we also calculated the confusion matrix and other accuracy metrics like the True Positive Rate, True Negative Rate, False Positive Rate, False Negative Rate, and the F1-score.

The True positive rate (also known as Sensitivity, Recall) (equation 1) and true negative rate (also known as Specificity) (equation 2) are performance metrics that are used to assess a model's accuracy in accurately detecting positive and negative instances. The number of genuinely negative instances identified as positive by the model are known as false positives (FP) (equation 3). The number of cases that are genuinely positive but are categorized as negative by the model are known as false negatives (FN) (equation 4).

$$TPR (= Recall) = \frac{True\ Positives}{True\ Positives + False\ Negatives} \quad (1)$$

$$TNR = \frac{True\ Negatives}{True\ Negatives + False\ Positives} \quad (2)$$

$$FPR = \frac{False\ Positives}{True\ Negatives + False\ Positives} \quad (3)$$

$$FNR = \frac{False\ Negatives}{True\ Positives + False\ Negatives} \quad (4)$$

The F1-score (equation 6) is the harmonic mean of precision (equation 5) and recall (equation 1), and it is used to balance the precision-to-recall trade-off. Precision is the number of correct positive predictions produced by the model out of all correct positive predictions made by the model, and recall is the number of correct positive predictions made out of all correct positive occurrences.

$$Precision = \frac{True\ Positives}{True\ Positives + False\ Positives} \quad (5)$$

$$F1\text{-score} = 2 \cdot \frac{Precision \cdot Recall}{Precision + Recall} \quad (6)$$

In Figure S3, we see the confusion matrix and the respective scores of the TPR, TNR, FPR, FNR, and F1-score of both Italy and the US Pacific Northwest.

References

- [1] Martin Klose. *Landslide databases as tools for integrated assessment of landslide risk*. Springer, 2015.
- [2] Melanie J Froude and David N Petley. Global fatal landslide occurrence from 2004 to 2016. *Natural Hazards and Earth System Sciences*, 18(8):2161–2181, 2018.
- [3] Eduardo Simoes and Gabriel Araujo. Death toll from brazil floods, landslides reaches 57. *Reuters*.
- [4] Aljazeera. Deadly landslide strikes southern peru amid heavy rainfall. *AL JAZEERA AND NEWS AGENCIES*.
- [5] Lucy Craymer and Lincoln Feast. New zealand declares national emergency as cyclone gabrielle wreaks havoc. *Reuters*.
- [6] Jente Broeckx, Mauro Rossi, Kobe Lijnen, Benjamin Campforts, Jean Poesen, and Matthias Vanmaercke. Landslide mobilization rates: A global analysis and model. *Earth-Science Reviews*, 201:102972, 2020.
- [7] Ugur Ozturk, Elisa Bozzolan, Elizabeth A Holcombe, Roopam Shukla, Francesca Pianosi, and Thorsten Wagener. How climate change and unplanned urban sprawl bring more landslides, 2022.
- [8] Xuanmei Fan, Ali P Yunus, Gianvito Scaringi, Filippo Catani, Srikrishnan Siva Subramanian, Qiang Xu, and Runqui Huang. Rapidly evolving controls of landslides after a strong earthquake and implications for hazard assessments. *Geophysical Research Letters*, 48(1):e2020GL090509, 2021.
- [9] Stefano Luigi Gariano and Fausto Guzzetti. Landslides in a changing climate. *Earth-Science Reviews*, 162:227–252, 2016.
- [10] Pedro Lima, Stefan Steger, Thomas Glade, and Martin Mergili. Conventional data-driven landslide susceptibility models may only tell us half of the story: Potential underestimation of landslide impact areas depending on the modeling design. *Geomorphology*, page 108638, 2023.
- [11] Jordi Corominas, Cees van Westen, Paolo Frattini, Leonardo Cascini, J-P Malet, Stavroula Fotopoulou, Filippo Catani, M Van Den Eeckhaut, Olga Mavrouli, Federico Agliardi, et al. Recommendations for the quantitative analysis of landslide risk. *Bulletin of engineering geology and the environment*, 73:209–263, 2014.
- [12] Fausto Guzzetti, Alessandro Cesare Mondini, Mauro Cardinali, Federica Fiorucci, Michele Santangelo, and Kang-Tsung Chang. Landslide inventory maps: New tools for an old problem. *Earth-Science Reviews*, 112(1-2):42–66, 2012.
- [13] Oldrich Hungr, Serge Leroueil, and Luciano Picarelli. The varnes classification of landslide types, an update. *Landslides*, 11(2):167–194, 2014.

- [14] DJ Varnes. Slope movement types and processes, in schuster, rl and krizek, rj ed. landslides-analysis and control. *TRB Special Report*, 176:11–33, 1978.
- [15] Kyle Bradley, Rishav Mallick, Harisma Andikagumi, Judith Hubbard, Ella Meilianda, Adam Switzer, Nairong Du, Gilles Brocard, Dedy Alfian, Benazir Benazir, et al. Earthquake-triggered 2018 palu valley landslides enabled by wet rice cultivation. *Nature Geoscience*, 12(11):935–939, 2019.
- [16] Franck Bourrier, Luuk Dorren, and Oldrich Hungr. The use of ballistic trajectory and granular flow models in predicting rockfall propagation. *Earth Surface Processes and Landforms*, 38(4):435–440, 2013.
- [17] Fausto Guzzetti, Paola Reichenbach, Francesca Ardizzone, Mauro Cardinali, and Mirco Galli. Estimating the quality of landslide susceptibility models. *Geomorphology*, 81(1-2):166–184, 2006.
- [18] Luigi Lombardo and P Martin Mai. Presenting logistic regression-based landslide susceptibility results. *Engineering geology*, 244:14–24, 2018.
- [19] Mauro Rossi, Fausto Guzzetti, Paola Reichenbach, Alessandro Cesare Mondini, and Silvia Peruccacci. Optimal landslide susceptibility zonation based on multiple forecasts. *Geomorphology*, 114(3):129–142, 2010.
- [20] Faming Huang, Haowen Xiong, Chi Yao, Filippo Catani, Chuangbing Zhou, and Jinsong Huang. Uncertainties of landslide susceptibility prediction considering different landslide types. *Journal of Rock Mechanics and Geotechnical Engineering*, 2023.
- [21] Dalia Bach Kirschbaum, Robert Adler, Yang Hong, Stephanie Hill, and Arthur Lerner-Lam. A global landslide catalog for hazard applications: method, results, and limitations. *Natural Hazards*, 52:561–575, 2010.
- [22] Paola Reichenbach, Mauro Rossi, Bruce D Malamud, Monika Mihir, and Fausto Guzzetti. A review of statistically-based landslide susceptibility models. *Earth-science reviews*, 180:60–91, 2018.
- [23] Mathieu Fressard, Yannick Thiery, and O Maquaire. Which data for quantitative landslide susceptibility mapping at operational scale? case study of the pays d’auge plateau hillslopes (normandy, france). *Natural Hazards and Earth System Sciences*, 14(3):569–588, 2014.
- [24] Tapas R Martha, Norman Kerle, Victor Jetten, Cees J van Westen, and K Vinod Kumar. Characterising spectral, spatial and morphometric properties of landslides for semi-automatic detection using object-oriented methods. *Geomorphology*, 116(1-2):24–36, 2010.
- [25] John Barlow, Steven Franklin, and Yvonne Martin. High spatial resolution satellite imagery, dem derivatives, and image segmentation for the detection of mass wasting processes. *Photogrammetric Engineering and Remote Sensing*, 72(6):687 – 692, 2006. Cited by: 102; All Open Access, Hybrid Gold Open Access.
- [26] Gabriele Amato, Lorenzo Palombi, and Valentina Raimondi. Data-driven classification of landslide types at a national scale by using artificial neural networks, 2021.
- [27] Pek Y Lum, Gurjeet Singh, Alan Lehman, Tigran Ishkanov, Mikael Vejdemo-Johansson, Muthu Alagappan, John Carlsson, and Gunnar Carlsson. Extracting insights from the shape of complex data using topology. *Scientific reports*, 3(1):1–8, 2013.
- [28] Yunan Luo. Sensing the shape of functional proteins with topology. *Nature Computational Science*, pages 1–2, 2023.
- [29] Gunnar Carlsson. Topological methods for data modelling. *Nature Reviews Physics*, 2(12):697–708, 2020.
- [30] Yuanwen Han and Xueying Bao. Topological mapping of complex networks from high slope deformation time series for landslide risk assessment. *Expert Systems with Applications*, 206:117816, 2022.
- [31] Farzad Zangeneh-Nejad and Romain Fleury. Topological analog signal processing. *Nature communications*, 10(1):2058, 2019.
- [32] ESRI. Arcgis - world shaded relief, 2020.
- [33] Guillaume Tuzin, Umberto Lupo, Lewis Tunstall, Julian Burella Pérez, Matteo Caorsi, Anibal M Medina-Mardones, Alberto Dassatti, and Kathryn Hess. giotto-tda: A topological data analysis toolkit for machine learning and data exploration. *The Journal of Machine Learning Research*, 22(1):1834–1839, 2021.
- [34] Gunnar Carlsson. Topology and data. *Bulletin of the American Mathematical Society*, 46(2):255–308, 2009.
- [35] Elizabeth Munch. A user’s guide to topological data analysis. *Journal of Learning Analytics*, 4(2):47–61, 2017.
- [36] Adélie Garin and Guillaume Tuzin. A topological" reading" lesson: Classification of mnist using tda. In *2019 18th IEEE International Conference On Machine Learning And Applications (ICMLA)*, pages 1551–1556. IEEE, 2019.

- [37] Felix Hensel, Michael Moor, and Bastian Rieck. A survey of topological machine learning methods. *Frontiers in Artificial Intelligence*, 4:52, 2021.
- [38] Peter Bubenik and Paweł Dłotko. A persistence landscapes toolbox for topological statistics. *Journal of Symbolic Computation*, 78:91–114, 2017.
- [39] Jan Reininghaus, Stefan Huber, Ulrich Bauer, and Roland Kwitt. A stable multi-scale kernel for topological machine learning. In *Proceedings of the IEEE conference on computer vision and pattern recognition*, pages 4741–4748, 2015.
- [40] Henry Adams, Tegan Emerson, Michael Kirby, Rachel Neville, Chris Peterson, Patrick Shipman, Sofya Chepushanova, Eric Hanson, Francis Motta, and Lori Ziegelmeier. Persistence images: A stable vector representation of persistent homology. *Journal of Machine Learning Research*, 18, 2017.
- [41] Ian Barnett, Nishant Malik, Marieke L Kuijjer, Peter J Mucha, and Jukka-Pekka Onnela. Endnote: Feature-based classification of networks. *Network Science*, 7(3):438–444, 2019.
- [42] Gérard Biau and Erwan Scornet. A random forest guided tour. *Test*, 25(2):197–227, 2016.
- [43] Leo Breiman. Random forests. *Machine learning*, 45(1):5–32, 2001.
- [44] Miron Bartosz Kurska. Robustness of random forest-based gene selection methods. *BMC bioinformatics*, 15(1):8, 2014.
- [45] Archana Chaudhary, Savita Kolhe, and Raj Kamal. An improved random forest classifier for multi-class classification. *Information Processing in Agriculture*, 3(4):215–222, 2016.
- [46] Ahmad Taher Azar, Hanaa Ismail Elshazly, Aboul Ella Hassanien, and Abeer Mohamed Elkorany. A random forest classifier for lymph diseases. *Computer methods and programs in biomedicine*, 113(2):465–473, 2014.
- [47] Mariana Belgiu and Lucian Drăguț. Random forest in remote sensing: A review of applications and future directions. *ISPRS journal of photogrammetry and remote sensing*, 114:24–31, 2016.
- [48] Alireza Arabameri, Subodh Chandra Pal, Fatemeh Rezaie, Rabin Chakraborty, Asish Saha, Thomas Blaschke, Mariano Di Napoli, Omid Ghorbanzadeh, and Phuong Thao Thi Ngo. Decision tree based ensemble machine learning approaches for landslide susceptibility mapping. *Geocarto International*, pages 1–35, 2021.
- [49] Oleg Okun and Helen Priisalu. Random forest for gene expression based cancer classification: overlooked issues. In *Iberian conference on pattern recognition and image analysis*, pages 483–490. Springer, 2007.
- [50] Max Kuhn, Kjell Johnson, et al. *Applied predictive modeling*, volume 26. Springer, 2013.
- [51] Cha Zhang and Yunqian Ma. *Ensemble machine learning: methods and applications*. Springer, 2012.
- [52] Abby R Kenigsberg, Jacques Rivière, Chris Marone, and Demian M Saffer. Evolution of elastic and mechanical properties during fault shear: The roles of clay content, fabric development, and porosity. *Journal of Geophysical Research: Solid Earth*, 125(3):e2019JB018612, 2020.
- [53] F Catani, N Casagli, L Ermini, G Righini, and G Menduni. Landslide hazard and risk mapping at catchment scale in the arno river basin. *Landslides*, 2:329–342, 2005.
- [54] Kamal Rana, Ugur Ozturk, and Nishant Malik. Landslide geometry reveals its trigger. *Geophysical Research Letters*, 48(4):e2020GL090848, 2021.
- [55] Faith E Taylor, Bruce D Malamud, Annette Witt, and Fausto Guzzetti. Landslide shape, ellipticity and length-to-width ratios. *Earth Surface Processes and Landforms*, 43(15):3164–3189, 2018.
- [56] CP Stark and F Guzzetti. Landslide rupture and the probability distribution of mobilized debris volumes. *Journal of Geophysical Research: Earth Surface*, 114(F2), 2009.
- [57] Gregor Luetzenburg, Kristian Svennevig, Anders A Bjørk, Marie Keiding, and Aart Kroon. A national landslide inventory for denmark. *Earth System Science Data*, 14(7):3157–3165, 2022.
- [58] Xuanmei Fan, Gianvito Scaringi, Guillem Domènech, Fan Yang, Xiaojun Guo, Lanxin Dai, Chaoyang He, Qiang Xu, and Runqiu Huang. Two multi-temporal datasets that track the enhanced landsliding after the 2008 wenchuan earthquake. *Earth System Science Data*, 11(1):35–55, 2019.
- [59] Tolga Görüm. Landslide recognition and mapping in a mixed forest environment from airborne lidar data. *Engineering Geology*, 258:105155, 2019.
- [60] Sean R LaHusen, Alison R Duvall, Adam M Booth, A Grant, Ben A Mishkin, David R Montgomery, William Struble, Joshua J Roering, and Joseph Wartman. Rainfall triggers more deep-seated landslides than cascadia earthquakes in the oregon coast range, usa. *Science Advances*, 6(38):eaba6790, 2020.

- [61] JJ Franczyk, WJ Burns, and NC Calhoun. Statewide landslide information database for oregon release-4.0, slido 4.0, 2019.
- [62] Xuanmei Fan, Gianvito Scaringi, Oliver Korup, A Joshua West, Cees J van Westen, Hakan Tanyas, Niels Hovius, Tristram C Hales, Randall W Jibson, Kate E Allstadt, et al. Earthquake-induced chains of geologic hazards: Patterns, mechanisms, and impacts. *Reviews of geophysics*, 57(2):421–503, 2019.
- [63] Benjamin B Mirus, Joel B Smith, and Rex L Baum. Hydrologic impacts of landslide disturbances: implications for remobilization and hazard persistence. *Water Resources Research*, 53(10):8250–8265, 2017.
- [64] Andrew J Pearce and Alex John Watson. Effects of earthquake-induced landslides on sediment budget and transport over a 50-yr period. *Geology*, 14(1):52–55, 1986.
- [65] Amy E East and Joel B Sankey. Geomorphic and sedimentary effects of modern climate change: current and anticipated future conditions in the western united states. *Reviews of Geophysics*, 58(4):e2019RG000692, 2020.
- [66] Yaspal Sundriyal, Vipin Kumar, Neha Chauhan, Sameeksha Kaushik, Rahul Ranjan, and Mohit K Punia. Brief communication on the nw himalayan towns; slipping towards potential disaster. *Natural Hazards and Earth System Sciences Discussions*, pages 1–9, 2023.
- [67] Antoine Dille, Olivier Dewitte, Alexander L Handwerker, Nicolas d’Oreye, Dominique Derauw, Gloire Ganza Bamulezi, Guy Ilombe Mawe, Caroline Michellier, Jan Moeyersons, Elise Monsieurs, et al. Acceleration of a large deep-seated tropical landslide due to urbanization feedbacks. *Nature Geoscience*, pages 1–8, 2022.
- [68] Johnny Alexander Vega and Cesar Augusto Hidalgo. Quantitative risk assessment of landslides triggered by earthquakes and rainfall based on direct costs of urban buildings. *Geomorphology*, 273:217–235, 2016.
- [69] Sid Perkins. Death toll from landslides vastly underestimated. *Nature News*, 8, 2012.
- [70] Michael Dietze, Solmaz Mohadjer, Jens M Turowski, Todd A Ehlers, and Niels Hovius. Seismic monitoring of small alpine rockfalls—validity, precision and limitations. *Earth Surface Dynamics*, 5(4):653–668, 2017.
- [71] Ionut Cristi Nicu, Luigi Lombardo, and Lena Rubensdotter. Preliminary assessment of thaw slump hazard to arctic cultural heritage in nordenskiöld land, svalbard. *Landslides*, 18(8):2935–2947, 2021.
- [72] Jose Frey-Martínez, Joe Cartwright, and David James. Frontally confined versus frontally emergent submarine landslides: A 3d seismic characterisation. *Marine and Petroleum Geology*, 23(5):585–604, 2006.
- [73] Alessandro Trigila, Carla Iadanza, and Daniele Spizzichino. Quality assessment of the italian landslide inventory using gis processing. *Landslides*, 7(4):455–470, 2010.
- [74] David Milne Cruden. Cruden, dm, varnes, dj, 1996, landslide types and processes, transportation research board, us national academy of sciences, special report, 247: 36-75. *Landslides Eng. Pract*, 24:20–47, 1996.
- [75] A Bashfield and A Keim. Continent-wide dem creation for the european union. In *34th international symposium on remote sensing of environment. the GEOSS era: Towards operational environmental monitoring. sydney, australia*, pages 10–15, 2011.
- [76] SL Slaughter, WJ Burns, KA Mickelson, KE Jacobacci, Alyssa Biel, and TA Contreras. Protocol for landslide inventory mapping from lidar data in washington state. *Washington Geological Survey Bulletin*, 82(27):3, 2017.
- [77] William J Burns and Ian Madin. Protocol for inventory mapping of landslide deposits from light detection and ranging (lidar) imagery. 2009.
- [78] William J Burns and Katherine A Mickelson. Protocol for deep landslide susceptibility mapping. 2016.
- [79] David M Cruden, David J Varnes, AK Turner, and RL Schuster. Landslides: investigation and mitigation. *Transportation research board special report*, 247:36–75, 1996.
- [80] Nicholas J Roberts and Stephen G Evans. The gigantic seymareh (saidmarreh) rock avalanche, zagros fold–thrust belt, iran. *Journal of the Geological Society*, 170(4):685–700, 2013.
- [81] SG Evans, MJ Bovis, and JN Hutchinson. Landslides of the flow type. *Environmental & Engineering Geoscience*, 7(3):221–238, 2001.